Half graben inversion tectonics revealed by gravity modeling in the Mikawa Bay Region, Central Japan

Ayumu Miyakawa [1]

Corresponding author

Email: miyakawa-a@aist.go.jp

Tomoya Abe [1]

Email: tomoya-abe@aist.go.jp

Tatsuya Sumita [1]

Email: t.sumita@aist.go.jp

Makoto Otsubo [1]

Email: otsubo-m@aist.go.jp

(Institutional addresses)

[1] Geological Survey of Japan, AIST, AIST Tsukuba Central 7, 1-1-1 Higashi, Tsukuba, Ibaraki Pref., 305-8567, Japan

Abstract

The Mikawa Bay Region, central Japan, is characterized by many active faults recording Quaternary activity. It is, however, difficult to understand the overall tectonic character of the region due to the thick sediments in this region. We estimated the depth and the structure of the basement top in the Mikawa Bay Region through the analysis of gravity data, compiling publicly available gravity data and our own gravity measurements in the central part of the region. The gravity basement map shows the deepening of the basement top from the Nishi-Mikawa Plain to the Chita Peninsula. Two-dimensional modeling constrains the orientation of the Utsumi and Takahama faults. The fact that the basement top structure related to the Kou Fault is insignificant in the gravity data indicates that the geometry of the Kou Fault is small relative to that of the Utsumi Fault. The basement top structure from the Nishi-Mikawa Plain to the Chita Peninsula reveals a half graben structure bounded by the Utsumi Fault. The inverse motion of the Utsumi Fault, which underwent normal faulting during the Miocene followed by recent reverse faulting, is interpreted to reflect the inversion tectonics of the half graben. The timing of the inversion tectonics, i.e. the reverse faulting of the Miocene normal fault, can be compared to an episode of basin inversion observed at the eastern margin of the Japan Sea, northeastern Japan. The Takahama Fault in the center of the

Nishi-Mikawa Plain is considered to have formed as a result of the backthrust of the Utsumi Fault under inversion tectonics. If the Takahama Fault is indeed the backthrust fault of the Utsumi Fault, the root of the Takahama Fault may be deep such that the Takahama Fault is seismogenic and linked to the 1945 Mikawa earthquake.

Keywords

Gravity survey, Inversion tectonics, Mikawa Bay Region, Nishi-Mikawa Plain, Chita Peninsula, Utsumi Fault, Takahama Fault, Basement structure, Half graben, Central Japan

Introduction

The Japan Arc is situation in a zone of plate convergence, where crustal dynamics such as earthquakes are common (Fig. 1 a). There are many active faults throughout the Japan Arc, many of which record Quaternary activity. This is the case in the Mikawa Bay Region, central Japan, close to the Chukyo area, which is one of the largest urban area in the country. The evaluation of fault activity is an important issue in Japan, however, it is difficult to understand the overall tectonic character of these active faults due to thick sediments and sea area in the Mikawa Bay Region. The Nishi-Mikawa Plain, a central part of the Mikawa Bay Region, is filled with the thick sedimentary rocks (~1000 m) formed during Neogene to Quaternary. The

Chita Peninsula, which exhibits recent dynamic topography at the western edge of the Mikawa Bay Region, is surrounded by the sea (i.e., Chita Bay, Mikawa Bay, and Ise Bay).

In this study, we focus on the geological structure of the Mikawa Bay Region in order to understand local fault dynamics. Several geological and geophysical studies have been previously undertaken for disaster mitigation in this region. Research conducted by the local government has revealed the basement structure beneath the plain and peninsula (Aichi Prefecture, 2001, 2002, 2003, 2004). The top of the basement sinks to the west, although basement rock are exposed in the eastern area of the plain. The deepest part of the basement lies beneath the Chita Peninsula, where its depth is greater than 1,500 m (Aichi Prefecture, 2003). Although active faults in the northwest part of the Nishi-Mikawa Plain and the northern part of the Chita Peninsula have been investigated using seismic reflection surveys to image their structures (Aichi Prefecture, 1997), the active faults in the central part of the Nishi-Mikawa Plain and the south part of Chita Peninsula remain under discussion. One such active fault, the Utsumi Fault, runs along the southwestern coast of the Chita Peninsula. Although the Utsumi Fault is expected to play an important role of the formation of the Chita Peninsula, it is currently poorly understood. Furthermore, a comprehensive understanding of the Takahama Fault, which distributes around a large urban area, has yet to be made.

In this study, we compiled existing gravity data together with our own gravity measurements in the northern part of the Mikawa Bay Region to image the structure of the basement beneath the Nishi-Mikawa Plain and Chita Peninsula. We revealed the orientation of the active fault in the central part of the Nishi-Mikawa Plain (i.e., the Takahama Fault) and along the southwestern edge of the Chita Peninsula (i.e., the Utsumi Fault). This allows a more thorough investigation of basement structure and fault dynamics in the Mikawa Bay Region.

Study area

The Mikawa Bay Region is located in the southern part of central Japan (Fig. 1 & 2). The Nishi-Mikawa Plain is in the northern Mikawa Bay Region, and the Chita Peninsula is at the west of the Nishi-Mikawa Plain, across Chita Bay. The Nishi-Mikawa Plain is mainly covered with Pleistocene terrace and alluvium deposits, and its topography is relatively flat (Makimoto et al., 2004). On the other hand, the Chita Peninsula has a relatively high topography. The hills of the Chita Peninsula approximately extend along N-S trend and primarily consist of Middle Pleistocene sediments (e.g., the Taketoyo and Noma formations) and Pliocene sedimentary rocks (the Tokai Group), whereas Miocene sedimentary rocks (the Morozaki Group) are exposed in the southern part of the peninsula (Kondo and Kimura, 1987). The Hazu Mountains and Mikawa Mountains, both of which consist of Mesozoic metamorphic rocks and granite, are located to the southeast and northeast of the

Nishi-Mikawa Plain, respectively. The Atsumi Peninsula is elongated in an ENE-WSW direction south of the Nishi-Mikawa Plain across Mikawa Bay. Ise Bay lies at the west of the Chita Peninsula. The largest plain closed to this region, the Nobi Plain, is distributed in the north of the Chita Peninsula.

Active fault occurs in and around the Nishi-Mikawa Plain and throughout the southern part of the Chita Peninsula (Fig. 2). In this paper, we focused on the two major active faults: the Utsumi and Takahama faults. The Utsumi Fault trends NW-EW along the southern edge of the Chita Peninsula (Fig. 2). The NE uplifting of the Utsumi Fault is recorded in subsurface Quaternary sediments discovered *via* shallow seismic reflection surveys (Chujo and Suda, 1971; 1972). This uplifting is believed to form the present topography of the southern Chita Peninsula. Gravity surveys around the southern part of the Chita Peninsula indicate a remarkably low Bouguer anomaly, suggesting thick sedimentary rocks and a deep basement top (Chujo and Suda, 1972). Deep seismic surveys able to image the shape of basement in this region have not yet been conducted. The Takahama Fault is a NW-SE trending active fault in the central Nishi-Mikawa Plain. Topographic features along the fault are, however, ambiguous in its southeastern part but clear in the northwestern part. The southwest-dipping reverse fault was discovered by seismic surveys conducted in the northwest (Aichi Prefecture, 1997). Nonetheless, geophysical surveys, such as seismic surveys, have not yet been conducted in the southeastern part of the fault, with the exception of several boring surveys (e.g., Abe et al., 2019a; 2019b). The Kou Fault, another active in the research area, is a N-S trending and east dipping (45°E) reverse fault (Kondo and Kimura, 1987). Although the Kou Fault is thought to have been active at the southern end of the N-S Kagiya fault zone traversing the Chita Peninsula, its slip rate is unknown (The Headquarters for Earthquake Research Promotion, 2004). Some studies have classified the Kou Fault as estimated active fault which is not directly observed on the ground surface but is inferred from topography (Imaizumi et al., 2018).

The Mikawa earthquake (Mw. 6.6) occurred in the Mikawa Bay Region on January 13, 1945, causing more than 1,000 causalities (Iida, 1978). Kikuchi et al. (2003) analyzed seismograms from the time of the Mikawa earthquake and revealed that its source was a NW-SE trending reverse fault with a slight left-lateral component. The slip distribution mainly consisted of two asperities: one near the hypocenter and another, with which the heavily damaged area is well correlated, 10–15 km to the northwest (Kikuchi et al., 2003). Yamanaka (2004) reanalyzed the slip inversion using additional seismograms; this revised result also showed a large slip in the northwest part of the fault model. Several other studies concerning the Mikawa earthquake have noted the predominant role of N-S or E-W trending faults (i.e., the Yokosuka and Fukozu faults) in the southeast part of the Nishi-Mikawa Plain and the eastern part of the Mikawa Bay.

Ando (1974) interpreted the ground movements as observed geodetically in terms of a N-S striking fault. Takano and Kimata (2009) reexamined the ground deformation caused by the earthquake through removing interseismic deformation and coseismic deformation resulting from the 1944 Tonankai earthquake (Mw = 7.9), which occurred ~150 km southwest off the Mikawa Bay Region. The best fit to the data was obtained from two faults along the sections running north and south of the Yokosuka and Fukozu faults. Sugito and Okada (2004) compiled geomorphic and geologic features of the surface rupture associated with the earthquake, and suggested that nearly pure thrust faulting along the southern N-S trending section was the predominant mode of surface faulting during the earthquake. The two prevailing models (i.e., the NW-SE trending fault and the N-S trending fault) are not consistent, thus the structure of the source fault of the Mikawa earthquake is still under discussion.

Datasets

We used publicly available gravity datasets and obtained our own gravity data across the southwest part of the Takahama fault in the central Nishi-Mikawa Plain. Most of the Mikawa Bay Region is covered by the publicly available datasets (Earth Watch Safety Net Research Center, 2011; Geological Survey of Japan, 2013; Gravity Research Group in Southwest Japan,

2001) that we used for our analysis (Fig. 3a). Furthermore, in order to investigate the detailed structure of the southwest part of the Takahama fault, we conducted additional gravity surveys at 57 gravity stations (Supple. Table 1) using a Lacoste and Romberg gravimeter (G-304). The Virtual Reference Station (VRS) method using Trimble R10 was applied to determine the location of the gravity stations. Bouguer anomalies were calculated with standard corrections (GSJ Gravity Survey Group, 1989) for free-air, Bouguer, terrain and atmosphere, and normal gravity was removed in accordance with the Geodetic Reference System 1980 (GRS80). Terrain corrections were applied for a range of 60 km using the 30 m mesh terrain data compiled by Murata et al. (2018). The reduced density of 2.3 g/cm^3 was used to obtain the Bouguer anomaly. This reduced density was visually selected using the Nettleton method (Nettleton, 1939) and allows the removal of topographic effects arising from sedimentary rocks exposed in the Chita Peninsula and Nishi-Mikawa Plain (Fig. 3b).

We used datasets for the elevation of the basement top to constrain the basement structure compiled by Aichi Prefecture (2001; 2003), expressed in the literature (Yamada et al., 1984), and originally compiled in this study from boring data provide by Aichi Prefecture, Nishio City, and geological maps (National Institute of Advanced Industrial Science and Technology, 2020b) (Supple. Table 2).

Methods

We estimated the structure of the basement top (i.e., the thickness of the overlying sediments) in the Mikawa Bay Region by analyzing gravity anomaly data.

Gravity basement analysis

To investigate the structure of the basement top in the study area, we first estimated the regional trend of the Bouguer anomaly and obtained the optimal density contrast between the sediment/sedimentary rock and the basement rocks. Observed Bouguer anomaly contains mainly two components: regional trend originated by deep/large structure and local effects of the shallow geology. The regional trend of the Bouguer anomaly is caused by the deep/large structure such as subducting slab beneath Japan or the Moho structure of the region, thus the regional trend is usually observed by long wavelength components. On the other hand, shallow geological structure such as the distribution of different rock types or sediment thickness, which forms the focus of this study, produces short wavelength Bouguer anomaly characteristics. In the study region, rocks can be divided into two types based on density: lower-density sediments/sedimentary rocks, and higher-density basement rocks (i.e., granite and metamorphic rocks). Knowing the density contrast between these two types of rocks allows us to estimate the thickness of the sediments/sedimentary rock covering the basement rocks from the residual Bouguer anomaly after the removal of the regional trend.

The regional trend of the Bouguer anomaly (long wavelength components) and its optimal density contrasts are estimated based on the elevation of the basement observed in the borehole or outcrop. The observed Bouguer anomaly (g_{BA}) with suitable terrain correction can be explained as the summation of the regional trend ($g_{regional}$) and local effects (short wavelength component) ($g_{sediments}$).

$$g_{BA} = g_{sediments} + g_{regional}$$

The regional trend is assumed to be expressed by the polynomial curved surface as follows:

$$g_{regional} = f(x, y|s)$$

where x and y are coordinates in the rectangular coordinate system and s is the coefficient of the polynomial curved surface (f). The local effect is assumed to be derived from the density contrast between sediments/sedimentary rocks and basement rocks and the thickness of the sediments/sedimentary rocks. We modeled the effect of the sediments/sedimentary rock cover below sea level using an infinite horizontal plate:

$$g_{sediments} = -2\pi G\Delta\rho H$$

where G is the gravitational constant (6.674×10^{-11} m^3/kg·s^2), $\Delta\rho$ is the density constrast between the sediments/sedimentary rocks and the basement rocks, and H is the thickness of the sediments/sedimentary rocks below sea level (i.e., elevation of the basement top). Here, the equation required to express the observed Bouguer anomaly can be written as follows:

$$g_{BA} = -2\pi G\Delta\rho H + f(x, y|s)$$

We obtained the regional component of the polynomial curved surface together with the optimal density contrast by solving the least squares problem for the basement top elevation below sea level (H_i) at the boring site (x_i, y_i), and then the observed Bouguer anomaly at the site (g_{BAi}):

$$\sum_{i=1}^{N} [g_{BA\,i} + 2\pi G\Delta\rho H_i - f(x_i, y_i|s)] \to min$$

where N is the number of the sites at which the depth of the basement and the Bouguer anomaly is known. Minimizing the least square problem is achieved by finding the least square solution to the following simultaneous equations:

$$\begin{bmatrix} F_1 \\ F_2 \\ \vdots \\ F_N \end{bmatrix} = \begin{bmatrix} A_{11} & A_{12} & \cdots & A_{1M} & H_1 \\ A_{12} & A_{22} & \cdots & A_{2M} & H_2 \\ \vdots & \vdots & \vdots & \vdots & \vdots \\ A_{N1} & A_{N2} & \cdots & A_{NM} & H_N \end{bmatrix} \begin{bmatrix} s_1 \\ s_2 \\ \vdots \\ s_M \\ 2\pi G\Delta\rho \end{bmatrix}$$

where **A** is the function of the coordinate (x, y). This formula can be written in $\mathbf{F} = \mathbf{A}\mathbf{s}$. Then, the solution can be found by $\left(\mathbf{A}^{\mathrm{T}}\mathbf{A}\right)\mathbf{s} = \mathbf{A}^{\mathrm{T}}\mathbf{T}$.

We used 85 control points for the known elevation of the basement top. The elevation of the basement at some control points is higher than sea level. For these points, the effect of basement topography above sea level on the Bouguer anomaly should be eliminated by applying appropriate corrections (free-air, Bouguer, and terrain) to the typical density of basement rock (Fig. 4). Hence, we calculated the gravitational corrections for each point at which the basement top is above sea level, using a widely accepted reduced density of 2.67 g/cm^3 for granitic rocks. We calculated the corrections for the remainder of the points using a reduced density of 2.3 g/cm^3 according to the Nettleton method outlined above.

We solved the least square problem by using the 85 control points and setting a 3rd order polynomial curved function for the regional trend of the Bouguer anomaly (i.e., $f\left(x, y \mid s\right) = s_1 x^2 y^2 + s_2 x^2 y + s_3 x^2 + s_4 x y^2 + s_5 x y + s_6 x + s_7 y^2 + s_8 y + s_9$). Thereafter, we obtained the optimal density contrast as −0.376 g/cm^3 (i.e., a sediment density of 2.294 g/cm^3) (Fig. 5) with the coefficients of the 3rd order polynomial curved function (Table 1). The obtained optimal density is almost the same as the value set for the sediments/sedimentary rock justified by using the Nettleton method (2.3 g/cm^3). The regional trend of the Bouguer anomaly along the 3rd order polynomial curved surface is highest in the southeast region and gradually decreases toward the northwest (Fig. 3c). This regional trend is consistent with results reported in the Aichi Prefecture (2003) report. The estimation error at the control points is approximately ± 200 m according to the difference between the observed elevation and the calculated elevation of the basement top (Fig. 6).

Finally, we obtained a map of the basement top by extracting the regional trend from the observed Bouguer anomaly (Fig. 3d) and multiplying the constants of the infinite horizontal plate ($0.0158 = -2\pi G(-0.376)$) (Fig. 7).

Detailed modeling of the basement profile

The estimation of the elevation of the basement top assumes that the infinite horizontal plate is effective for determining the overall structure but unsuitable for the imaging non-flat structures (e.g., faults and slops). Hence, we conducted additional two-dimensional modeling to illuminate the detailed structure of the region, including the Utsumi and Takahama faults. We set a SW-NE trending survey line from the southwest of the Chita Peninsula to the central part of the Nishi-Mikawa Plain (Fig. 2b). The initial model was set as the profile of the gravity basement model estimated in the previous step. We then modified the initial model by adding the Utsumi and Takahama faults. Although we also attempted to model the Kou Fault crossing the survey line, we were unable to constrain the optimal solution because the gravity data lacked sufficient sensitivity on deep and minor structures related to this fault (see details in the Results). The validity of the model was evaluated by fitting the observed Bouguer anomaly, which is detrended off the regional trend. Gravity stations within 0.5 km onshore and 1.0 km offshore relative to the survey line were used. To select the best fit parameters, we employed the genetic algorithm (GA), a method for solving optimization problems based on a natural selection process that mimics biological evolution (e.g. Goldberg 1989). The GA which is able to solve non-linear global optimization problems is suitable to find the best parameter set in our model.

We obtained the optimal basement model as follows. The synthetic Bouguer anomaly was calculated from the initial model with estimated density contrast (−0.376 g/cm^3) *via* the two-dimensional Talwani method (Talwani and Bolt, 1973). Although the overall calculated Bouguer anomaly based on the initial model is consistent with the observed Bouguer anomaly, some discrepancy is observed, especially around the faulted areas (green line in Fig. 8). To reduce these discrepancies, we set parameters to modify the basement structure: the dip of the Utsumi Fault, the dip of the Takahama Fault, the depth shift in the southwest part of the region, the depth shift in the northeast part of the region, the tilt correction of the basement between the Chita Peninsula and Nishi-Mikawa Plain, and the position of the center of tilt correction. The dip of the Utsumi Fault in the deep basement is unknown because the depth of the seismic image across the Utsumi Fault is too shallow (~100 m in depth) to capture the shape of the basement (Chujo and Suda, 1971; 1972). Hence, we set the dip of the Utsumi Fault to range from 30°E to 30°W (i.e., 30° to 150° from the east). The dip of the southeast part of the Takahama Fault, through which the survey line passes, is also unknown, although the dip of the northwest part of the fault was estimated as 60°W by seismic surveys (Aichi Prefecture, 1997). Hence, we set the dip of the Utsumi Fault to range from 30°E to 30°W (i.e., 30° to 150° from the east). The tip (surface position) of the Utsumi and Takahama faults were fixed according to previous studies (Imaizumi et al., 2018; Abe et al., 2019a; 2019b); the tip of the Utsumi Fault was set at 0 km (i.e., with its origin in the horizontal direction), while the tip of the Takahama Fault was set at 22.98 km. Even in the flat basement, the synthetic Bouguer anomaly calculated from the initial model is systematically lower than the observed Bouguer anomaly. Therefore, we set the depth shift in the southwest part (−10 km–0 km in the horizontal direction) and the northeast part (22.98 km–30 km in the horizontal direction) to range from −0.2 km to 0.2km and −0.1 km to 0.1 km in the vertical direction, respectively. A tilt correction for the basement between the Chita Peninsula and the Nishi-Mikawa Plain ranging from −2° to 2°, and the center of the tilt correction ranging from 15 km to 18 km were also set to provide parameters that fit the lowest Bouguer anomaly observed in the Chita peninsula.

The synthetic Bouguer anomaly at the observation point calculated from a basement model with the parameters outlined above was calculated using the two-dimensional Talwani’s method. The parameter set which produces the best fit model was searched using the GA (Table 2; Fig. 8 & 9). To validate the robustness of the GA analysis, we ran the GA 10 times and obtained almost the same results every time, within the range of a few degrees or meters, which is considered sufficient accuracy for the following discussion (Suppl. Table 3). We selected the parameter set showing the lowest error from the 10 sets as the optimal parameter set (Table 2).

Results

Basement top structure around the Nishi-Mikawa Plain

The structure of the basement top around Mikawa Bay Region is depicted from the Bouguer anomaly (Fig. 7). The basement top is shallow at the east side of the Nishi-Mikawa Plain, consistent with the exposure of basement rocks in the Mikawa Mountains and Hazu Mountains eastward of the Nishi-Mikawa Plain. The basement top deepens from the Nishi-Mikawa Plain to the Chita Peninsula, where its depth is greater than 1,500 m. This trend is consistent with the results of the seismic survey conducted by Aichi Prefecture (2003). The depression of the basement beneath the Chita Peninsula continues to the north of the Nishi-Mikawa Plain.

The NWN-SEW trending shallow basement top in Ise Bay to the west of Chita Peninsula, which is thought to have been caused by reverse faulting of the Ise Bay Fault, is also consistent with previous studies (Okada et al., 2000). The basement top become considerable shallower to the west across the Utsumi Fault. Its depth in Ise Bay, far west of Chita Peninsula is, however, inconsistent with results obtained by the seismic reflection survey (Iwabuchi et al., 2000). This area, the Ise Bay far west of Chita Peninsula, is the west edge of our study field, where no boring sites were obtained to control basement top, thus the regional trend of the estimated Bouguer anomaly might be inappropriate in this region.

Fault-related basement top structure in the Mikawa Bay Region

The depth of the basement top drastically changes across the Utsumi Fault (Fig. 8 & 9). The orientation of the Utsumi Fault indicates that it is a normal fault with high dip angle (~70°E) and that the gap between the southwest foot wall and the northeast hanging wall is ~2000 m (Fig. 8). The Takahama Fault is a reverse fault with a dip angle of ~60°E. This dip is consistent with the observed fault dip in the northwestern part of the Takahama Fault (Aichi Prefecture, 2003). The gap between the hanging wall is ~200 m, which is relatively smaller than that of the Utsumi Fault. The basement top tilts and deepens from the Takahama Fault to the Utsumi Fault.

Basement top structure related to the Kou Fault

We attempted to incorporate the basement top structure of the Kou Fault by including the Kou Fault with a 45°E dip. It is, however, difficult to constrain the structure arising from the Kou Fault. Even when setting the opposite geometry to that of the basement (i.e., reverse fault and normal fault), both synthetic Bouguer anomalies calculated from the conflicting models are within the range of the observed Bouguer anomaly (Fig. 10). The gravitational signal from the resulting small, deep structure is dull, such that the signal of the basement top topography related to the Kou Fault cannot be constrained in our analysis. Hence, it was not possible to distinguish the basement top geometry related to the Kou Fault using gravity data. This suggests that basement top geometry related to the Kou Fault is relatively smaller than that relating to the Utsumi Fault.

Discussion

Inversion tectonics in the Mikawa Bay Region

The topographic features of the basement top depict a half graben structure beneath the Chita Peninsula. Depression of the basement top beneath the Chita Peninsula has been noted in previous studies (Aichi Prefecture, 2003; 2004; Chujo and Suda, 1972). We found that the Utsumi Fault is a normal fault with a large gap, and the tilted basement top forms the hanging wall of the Utsumi Fault (Fig. 8). These structural features correspond to a large half graben structure in the Mikawa Bay Region, where the Utsumi Fault is the edge fault of the half graben.

The geometry of the basement top and uplift forming the Chita Peninsula is caused by inversion tectonics of the half graben. A discrepancy between the recent reverse faulting and the depressed basement beneath the Chita Peninsula was identified in a previous study (Chujo and Suda, 1972). The recent NE side up reverse faulting (i.e., uplift of the Chita Peninsula side) is recorded in the Quaternary sediments. On the other hand, Miocene normal faulting of the Utsumi Fault is suggested from the thick Miocene sediments on the hanging wall (Aichi Prefecture, 2004). Therefore, the motion of the Utsumi Fault is shown to have changed from normal faulting in the Miocene to recent reverse faulting (Aichi Prefecture, 2004). This change of motion is interpreted as inversion tectonics related to the half graben structure discovered herein (Fig. 11).

The tectonic history of the Chita Peninsula has been reconstructed using the sediments/sedimentary rocks observed in the region. The thick Miocene sedimentary rocks (Morozaki Group) filled the hanging wall of the Utsumi Fault; hence the motion of the Utsumi Fault was normal in the Miocene (Aichi Prefecture, 2004). The half graben structure was formed during this extensional stage. Subsequently, Pliocene sedimentary rocks (Tokai Group) were folded before the Middle Pleistocene (Makinouchi, 2019). This may suggest that the region was under moderate compressional stress at this time, which also accounts for the fact that the Utsumi Fault was not reactivated during this stage. The Utsumi Fault reactivated as a reverse fault around 0.5 Ma (following the depositional age of the Middle Pleistocene

Taketoyo Formation) (Makinouchi, 2019). The displacement of the reverse faulting was, however, insufficient to recover the gap formed during normal faulting in the Miocene.

The tectonic history of the inversion structure in the Chita Peninsula is comparable to inversion tectonics at the eastern margin of the Japan Sea in northeast Japan. The inversion structures in the eastern margin of the Japan Sea are the most completely described example in Japan (e.g., Okamura, 1995; Morijiri, 1996). Normal faults were formed during the Early to Middle Miocene, and were reactivated in the Pliocene to Quaternary (Okamura, 1995). Periods of normal fault formation and reactivation in the eastern margin of Japan Sea in northeast Japan coincide with those in the Chita Peninsula. This episode of Miocene normal faulting is believed to be related to the opening of the Japan Sea, whereas the reactivation of reverse faulting motion is considered to be due to E-W compression resulting from the present tectonic setting. Although the tectonic history between central and northeast Japan differs after the opening of the Japan Sea (e.g., Hayashida et al., 1991; Jolivet et al., 1995; Lallemand Jolivet, 1986; Otofuji et al., 1985), the deduced agreement in the period of the inversion tectonics can be considered a clue to understanding the tectonic dynamics of the Japan Arc.

The Takahama Fault under inversion tectonics

Our results also enable us to discuss the role of the Takahama Fault in the inversion tectonic system in the Mikawa Bay Region. The Takahama Fault constitutes the NE edge of the half graben (Fig. 8 & 9). Its basement top is tilted from the Takahama Fault to the Utsumi Fault, although the basement top is almost flat northeast of the Takahama Fault. Concurrently, the orientation of the Takahama Fault (west dipping) is hanging wall-vergent. The Takahama Fault and the Utsumi Fault (east dipping) are in a conjugate relationship. Hanging wall-vergent thrusts (i.e., “backthrusts”) develop in analog inversion tectonics experiments (McClay and Buchanan, 1992) (Fig. 11a). Furthermore, fault traces of both the Takahama and Utsumi Fault observed on the ground surface are NW-SE trending, and both traces are parallel. Such parallel master normal fault and backthrust relationships are observed in three-dimensional analogue models reconstructing inversion tectonics (Yamada and McClay, 2003). These geometrical features suggest that the Takahama Fault is a backthrust of the Utsumi Fault, which is the master normal fault of the inversion structure.

The initiation of the reverse faulting period of the Takahama Fault also suggests a conjugate relationship with the reverse faulting of the Utsumi Fault. The initiation/acceleration period of the reverse faulting of the Takahama Fault is estimated to be late middle Pleistocene base on the analysis of boring cores around the southeastern part of the fault (Abe et al. 2019a; 2019b). This is similar period as that of the initiation of reverse faulting of the Utsumi Fault (Makinouchi, 2019). The simultaneity of the initiation of reverse faulting suggests that the

Takahama and Utsumi faults are parts of the same inversion tectonic system.

The deep extent of the Takahama Fault within the basement rock cannot be detected by the present gravity survey. However, if the Takahama Fault is the backthrust of the Utsumi Fault, it should reach seismogenic depths. The slip distribution of the 1945 Mikawa earthquake estimated by waveform inversions shows a large slip asperity on the NW-SE trending reverse fault (Kikuchi et al., 2003; Yamanaka, 2004). The location of the northwestern asperity is notably correlated with the heavily damaged area, consistent with deeper extension of the Takahama Fault (~10 km depth). The strike of the Takahama Fault (N45°W) is parallel to the fault model of the 1945 Mikawa earthquake described by Kikuchi et al. (2003); moreover, the tips of the fault traces are significantly correlated. This agreement suggest that the deep extension of the Takahama Fault can explain the fault model of the northwestern asperity described in Kikuchi et al. (2003) and Yamanaka, 2004. The dip of the fault model (30°W) in these studies is, however, lower than the dip estimated in this study (~60°W). This discrepancy may be solved by assuming listric fault geometry in the deeper portion of the Takahama Fault. Based on the leveling data taken by local goverment, the 40 cm subsidence of the footwall side (NE side) relative to the hanging wall side along the Takahama Fault in the 1945 Mikawa earthquake (Iida and Sakabe, 1972) supports evidence for reverse faulting of the Takahama Fault during the earthquake. On the other hand, several studies suggest that the N-S trending reverse faults in the southwest ward of the Nishi-Mikawa Plain (i.e., the Yokosuka and Fukouzu fsults) were predominant factors in surface faulting during the earthquake (e.g., Ando 1974, Sugito and Okada, 2004; Takano and Kimata, 2009). Therefore, the deep extension of the Takahama Fault, the back thrust of the Utsumi Fault, may be one possible source fault for the 1945 Mikawa earthquake, but this remains difficult to unambiguously conclude.

Conclusions

We analyzed gravity data to describe the basement top structure in the Mikawa Bay Region. The gravity basement map showed the deepening of the basement top from the Nishi-Mikawa Plain to the Chita Peninsula. Two-dimensional modeling constrained the orientation of the Utsumi and Takahama faults, although the basement top structure related to the Kou Fault is so minor that the gravity data cannot constrain it. The basement top structure from the Nishi-Mikawa Plain to the Chita Peninsula revealed a half graben structure defined by the Utsumi Fault. The inverse motion of the Utsumi Fault, which underwent normal faulting during the Miocene and recent reverse faulting, is interpreted in terms of the inversion tectonics of the half graben. These inversion tectonics, reflecting the reverse faulting of the Miocene normal fault, are comparable to the basin inversion observed at the eastern margin of the Japan Sea in northeastern Japan. The Takahama Fault in the northwestern part of the Nishi-Mikawa Plain is considered to have formed during the backthrust of the Utsumi Fault under inversion tectonics. If the Takahama Fault is indeed the backthrust fault of the Utsumi Fault, the root of the Takahama Fault may be so deep as to reach the seismogenic zone, suggesting that the Takahama Fault may be the source fault of the 1945 Mikawa earthquake.

Abbreviations

GA: Genetic algorithm

Declarations

Availability of data and material

The dataset supporting the conclusions of this article is included within the article and its additional file. Some datasets is available in the cited database in the article.

Competing interests

The authors declare that they have no competing interest.

Funding

(not applicable)

Authors' contributions

AM conducted the gravity observation, analysis and designed the study. TA proposed the topic and supported to compile related information. TS proposed the plan of the analysis and supported the analysis. MO collaborated with the corresponding author in the construction of manuscript. All authors read and approved the final manuscript.

Acknowledgements

We are grateful to T. Komatsubara, T. Sato, S. Okuma and R. Nakashima (Geological survey of Japan, AIST) for their support for our project. The GNSS data were analyzed by Y. Takahashi, who is the staffs of Geological Survey of Japan, AIST. Prof. H. Hoshi (Aichi University of Education) gives us impressive comments. Some figures were generated using Generic Mapping Tools (Wessel et al., 2013). We appreciate Aichi Prefecture and Nishio City

offering their boring data.

References

Abe T, Nakashima R, Naya T (2019a) Reports of coring survey in Aburagafuchi Lowland, southwestern part of Nishimikawa Plain, central Japan. GSJ Interim Report 79: 173–186. (in Japanese with English abstract)

Abe T, Nakashima R, Naya T, Mizuno K (2019b) Subsurface geology along the Takahama Fault in the southwestern part of the Nishimikawa Plain. Annual Meeting of the Association of Japanese Geographers, Autumn 2019, The Association of Japanese Geographers. (in Japanese) https://doi.org/10.14866/ajg.2019a.0_172

Aichi Prefecture (2002) Subsurface Survey Report of Sedimentary Basin under the Mikawa Plain. Aichi Prefecture in 2002, Nagoya. (in Japanese)

Aichi Prefecture (2003) Subsurface Survey Report of Sedimentary Basin under the Mikawa Plain. Aichi Prefecture in 2003, Nagoya. (in Japanese)

Aichi Prefecture (2004) Subsurface Survey Report of Sedimentary Basin under the Mikawa Plain. Aichi Prefecture in 2004, Nagoya. (in Japanese)

Aichi Prefecture (2005) Subsurface Survey Report of Sedimentary Basin under the Mikawa Plain. Aichi Prefecture in 200, Nagoya. (in Japanese)

Ando M (1974) Faulting in the Mikawa earthquake of 1945. Tectonophysics 22(1–2):173–186. https://doi.org/10.1016/0040-1951(74)90040-7

Chujo J, Suda Y (1971) Gravitational survey of northern Ise Bay. Bull Geol Surv Jpn 22(8):415–435. (in Japanese with English abstract)

Chujo J, Suda Y (1972) Gravitational survey of southern Ise Bay and Mikawa Bay. Bull Geol Surv Jpn 23(10):573–594. (in Japanese with English abstract)

Fire and Disaster Prevention Office, General Affairs Department, Aichi Prefecture (1996) Report on the research on the activity of active faults in the North Chita and the Kinuura Areas. Aichi Prefecture, Nagoya. (in Japanese)

Geological Survey of Japan (2013) Gravity Database of Japan. DVD edition, Digital Geoscience Map P-2. Geological Survey of Japan, AIST, Tsukuba.

Goldberg DE (1989) Genetic algorithms in search, optimization, and machine learning. Addison-Wesley, Boston.

Gravity Research Group in Southwest Japan (2001) Gravity database of Southwest Japan (CD-ROM). Bull Nagoya University Museum, Special Report No. 9, Nagoya University Museum, Nagoya.

GSJ Gravity Survey Group (1989) On the standard procedure SPECG1988 for evaluating the correction of gravity at the Geological Survey of Japan. Bull Geol Surv Jpn 40(11):601–611. (in Japanese with English abstract)

Hayashida A, Fukui T, Torii M (1991) Paleomagnetism of the Early Miocene Kani Group in southwest Japan and its implication for the opening of the Japan Sea. Geophys Res Lett 18(6):1095–1098. https://doi.org/10.1029/91GL01349

Iida K (1978) Distribution of the Earthquake damage and Seismic Intensity caused by the Mikawa earthquake of January 13, 1945. Report of the Earthquake Section of Disaster Prevention Committee of Aichi Prefecture. Aichi Prefecture, Nagoya. (in Japanese)

Iida K., Sakabe K. (1972) The extension of the Fukozu fault associated with the Mikawa earthquake in 1945. Zisin, 24, 44-55. (in Japanese with English abstract)

Imaizumi T, Miyauchi T, Tsutsumi H, Nakata T (2018) Digital active fault map of Japan. University of Tokyo Press, Tokyo. (in Japanese)

Iwabuchi Y, Nishikawa H, Noda N, Kawajiri C, Nakagawa M, Aoto S, Kato I, Amma K, Nagata S, Kadoya M (2000) Active faults surveys in the Ise Bay. Rep Hydrogr Res 36:73–96. (in Japanese with English abstract)

Jolivet L, Shibuya H, Fournier M (1995) Paleomagnetic rotations and the Japan Sea opening. In: Taylor B, Natland J (eds) Active margins and marginal basins of the western Pacific. Geophysical Monograph Series, vol 88. American Geophysical Union, Washington, D. C., pp 355–369. https://doi.org/10.1029/GM088p0355

Kikuchi M, Nakamura M, Yoshikawa K (2003) Source rupture processes of the 1944 Tonankai earthquake and the 1945 Mikawa earthquake derived from low-gain seismograms. Earth Planets Space 55(4):159–172. https://doi.org/10.1186/BF03351745

Kondo Y, Kimura I (1987) Geology of the Morozaki district. With Geological Map of Japan 1:50,000, Morozaki. Geological Survey of Japan, Tsukuba. (in Japanese with English abstract)

Lallemand S, Jolivet L (1986) Japan Sea: a pull-apart basin? Earth Planet Sci Lett 76(3–4):375–389. https://doi.org/10.1016/0012-821X(86)90088-9

Makimoto H, Yamada N, Mizuno K, Takada A, Komazawa M, Sudo S (2004) Geological Map of Japan 1:200,000, Toyohashi and Irago Misaki. Geological Survey of Japan, Tsukuba. (in Japanese with English abstract)

Makinouchi T (2019) Active faults in Chita Peninsula and large earthquakes in the Nankai

Trough. Chita Peninsula: its history and present 23:1–20. (in Japanese)

McClay KR, Buchanan PG (1992) Thrust faults in inverted extensional basins. In: McClay KR (ed) Thrust tectonics. Springer, Dordrecht, pp 93–104. https://doi.org/10.1007/978-94-011-3066-0_8

Morijiri R (1996) Subsurface structure of the southeastern margin of the Japan Sea inferred from Bouguer gravity anomalies. Zishin (J Seismol Soc Jpn 2nd ser) 49(3):403–416. https://doi.org/10.4294/zisin1948.49.3_403 (in Japanese with English abstract)

Murata Y, Miyakawa A, Komazawa M, Nawa K, Okuma S, Joshima M, Nishimura K, Kishimoto K, Miyazaki T, Shichi R, Honda R, Sawada A (2017) Gravity Map of Kanazawa District, Gravity Map Series (Bouguer Anomalies) 33. Geological Survey of Japan, AIST, Tsukuba. (in Japanese with English abstract)

National Institute of Advanced Industrial Science and Technology (2020a) Active Fault Database of Japan, Research Information Database DB095, National Institute of Advanced Industrial Science and Technology.

https://gbank.gsj.jp/activefault/index_e_gmap.html. Accessed 22 Apr 2020

National Institute of Advanced Industrial Science and Technology (2020b) Seamless Digital Geological Map of Japan (1:200,000), https://gbank.gsj.jp/seamless/v2/viewer/?lang=en. Accessed 28 Apr 2020

Nettleton L. L. (1939) Determination of density for reduction of gravimeter observations. Geophysics, 4(3), 176-183.

Okada A, Toyokura I, Makinouchi T, Fujiwara Y, Ito T (2000) The Ise Bay Fault off the Chita Peninsula, Central Japan. J Geogr (Chigaku Zasshi) 109(1):10–26. https://doi.org/10.5026/jgeography.109.10 (in Japanese with English abstract)

Okamura Y, Watanabe M, Morijiri R, Satoh M (1995) Rifting and basin inversion in the eastern margin of the Japan Sea. Isl Arc 4(3):166-181. https://doi.org/10.1111/j.1440-1738.1995.tb00141.x

Otofuji YI, Matsuda T, Nohda S (1985) Opening mode of the Japan Sea inferred from the palaeomagnetism of the Japan Arc. Nature 317(6038):603–604. https://doi.org/10.1038/317603a0

Sugito N, Okada A (2004) Surface rupture associated with the 1945 Mikawa earthquake. Active Fault Res 24:103–127. https://doi.org/10.11462/afr1985.2004.24_103 (in Japanese with English abstract)

Takano K, Kimata F (2009) Re-examination of ground deformation and fault models of the 1945 Mikawa Earthquake (M = 6.8). Zisin (J Seismol Soc Jpn 2nd ser) 62(2+3):85–96. https://doi.org/10.4294/zisin.62.85 (in Japanese with English abstract)

Talwani M (1973) Computer usage in the computation of gravity anomalies. In: Bolt BA (ed) Geophysics. Method in Computational Physics, vol 13. Academic Press, New York, pp 343-389. https://doi.org/10.1016/B978-0-12-460813-9.50014-X

The Earthquake Research Committee (2004). Long-term evaluation of earthquake along the Byobu-yama and Ena-san active fault zone and Sanage-yama active fault zone. https://www.jishin.go.jp/regional_seismicity/rs_katsudanso/f053_054_byobu_ena_sanage/.

Accessed 24 Apr 2020 (in Japanese)

Wei D, Seno T (1998) Determination of the Amurian plate motion. In: Flower MFJ Chung SL, Lo CH, Lee TY (eds) Mantle dynamics and plate interactions in East Asia. Geodynamics Series, vol 27. American Geophysical Union, Washington D. C., pp 337–346. https://doi.org/10.1029/GD027p0337

Wessel P, Smith W. H. F., Scharroo R, Luis J and Wobbe F (2013) Generic mapping tools: Improved version released. EOS Trans AGU 94(45):409–410. doi:10.1002/2013EO450001.

Yamanaka Y (2004) Source rupture processes of the 1944 Tonankai earthquake and the 1945 Mikawa earthquake. The Earth Monthly 26(11):739–745. (in Japanese)

Yamada Y, McClay K (2004) 3-D analog modeling of inversion thrust structures. In: McClay KR (ed) Thrust Tectonics and Hydrocarbon Systems. AAPG Memoir, vol 82. American Association of Petroleum Geologists, Tulsa, pp 276–301. https://doi.org/10.1306/M82813C16

Yamamoto A, Shichi R, Kudo T (2011) Gravity database of Japan (CD-ROM). Special Publication No. 1. The Earth Watch Safety Net Research Center, Chubu University, Nagoya.

Yamada T, Takada Y, Yamada N, Asao K, Ohtomo Y (1984) A new fact on the location of the Median Tectonic Line around Cape Irago, Atsumi Peninsula, central Japan. The Journal of the Geological Society of Japan 90(12):915–918. https://doi.org/10.5575/geosoc.90.915 (in Japanese)

Figure 1. Map showing the tectonic setting of the Japanese islands (a) and the geology of the study area (b) (from National Institute of Advanced Industrial Science and Technology (2020b)). (a) Thick black lines represent plate boundaries and black arrows represent relative plate motions (after Wei and Seno, 1998). The blue rectangle represents the study area and the green shaded area is the eastern margin of the Japan Sea (see main text for discussion).

Figure 2. Topography and active faults in the Mikawa Bay Region. Red lines represent the traces of active faults in Figure 1(b) (National Institute of Advanced Industrial Science and Technology, 2020a). The blue line indicates the profile line shown in Figures 8, 9, and 10.

Figure 3. Bouguer anomaly of the study area. (a) Red dots indicate the location of gravity stations used for this analysis. (b) Bouguer anomaly calculated with a reduced density of 2.3 g/cm^3. (c) Regional trend of the Bouguer anomaly. Black dots and crosses represent the boring locations and basement exposing locations, respectively. (d) Residual Bouguer anomaly obtained by deducting the regional trend (c) from the original Bouguer anomaly (b).

Figure 4. Schematic diagrams showing the calculation of residual Bouguer anomalies at the boring sites and basement exposure points. (a) Definition of the elevation of points (h) and the density of the basement (ρ_b) and one unit of sediments/sedimentary rocks (ρ_s). The elevation of the buried basement top is represented by H. (b) Gravitational corrections (Δg) (Bouguer, free-air and terrain correction) are calculated using the density of the rock exposed at the observation points. g_n is normal gravity in accordance with the Geodetic Reference System 1980 (GRS80). The corrected Bouguer anomaly (g_{BA}) represents the Bouguer anomaly considered. (c) The residual Bouguer anomaly (g') is obtained by removing the

regional trend from the Bouguer anomaly (g_{BA}). The residual Bouguer anomaly must consist of the gravity anomaly from the thickness of the sediments/sedimentary rocks (i.e., the elevation of the basement top).

Figure 5. Relationship between the elevation of the basement and the residual Bouguer anomaly at the boring site or basement exposure (Fig. 4). The red line represents the calculated regression line.

Figure 6. Difference between the observed elevation of the basement top and the calculated elevation of the basement top (see Fig. 5).

Figure 7. Gravity basement map obtained using the relationship between the depth of the basement and the residual Bouguer anomaly (Fig. 5) based on the the residual Bouguer anomaly map (Fig. 3d).

Figure 8. Profiles of the Bouguer anomaly (a) and the topography of the basement top (b). (a) The observed and interpolated residual Bouguer anomalies are represented by the open circles and cyan line, respectively. The green line and red line represent the calculated Bouguer

anomaly from the initial model (green in b) and the optimum model (red in b) using the 2D Talwani’s method. (b) The green line represents the initial model extracted from the gravity basement model (Fig. 5) along the survey line. The red line represents the optimum basement model obtained by selecting the best parameters (see Table 2). The black line represents the elevation of the ground surface. The origin of the x-axis is set as the tip of the Utsumi Fault in both a and b.

Figure 9. Close-up views of the profiles of the Bouguer anomaly (a) and the topography of the basement top (b) around the Takahama Fault. The tip of the Takahama Fault is located at 22.98 km. (a) The observed and interpolated residual Bouguer anomalies are represented by open circles and the cyan line, respectively. The green line and red line represent the calculated Bouguer anomaly from the initial model (green in b) and the optimum model (red in b) using the 2D Talwani’s method. (b) The green line represents the initial model extracted from the gravity basement model (Fig. 5) along the survey line. The red line represents the optimum basement model obtained by selecting the best parameters (Table 2). The black line represents the elevation of the ground surface. The origin of the x-axis is set at the tip of the Utsumi Fault in both a and b.

Figure 10. Profiles of the Bouguer anomaly and the topography of the basement top with 600 m of displacement along the Kou Fault at 2.26 km with a dip of 45°E. (a) Reverse fault structure of the Kou Fault using the optimal basement model. (b) Normal fault structure of the Kou Fault using the optimal basement model. Lines and circles are same as shown in Figure 8. The origin of the x-axis is set at the tip of the Utsumi Fault in both a and b.

Figure 11. (a) Conceptual models for thrust faults developed by the dip-slip inversion of a normal fault system (modified after McClay and Buchanan, 1992). The white arrow represents normal faulting during the extensional stage. Black arrows indicate reverse faulting during the compressional stage following the extensional stage. (b) Conceptual models for the fault system across the Chita Peninsula and the Nishi-Mikawa Plain (not to scale). The white arrow represents the normal faulting in the extensional stage in Miocene. Black arrows indicate reverse faulting during the compressional stage following extensional stage in the Pliocene to Quaternary.

Table 1. Coefficient of the polynomial function representing the regional trend of the Bouguer anomaly.

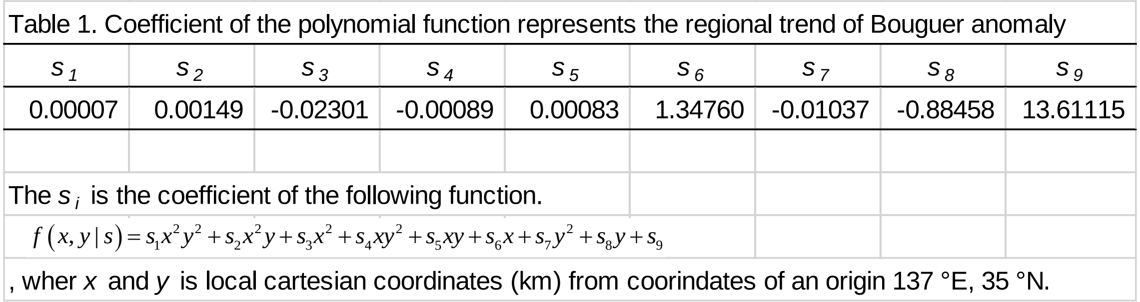

Table 1. Coefficient of the polynomial function represents the regional trend of Bouguer anomaly

s_1	s_2	s_3	s_4	s_5	s_6	s_7	s_8	s_9
0.00007	0.00149	-0.02301	-0.00089	0.00083	1.34760	-0.01037	-0.88458	13.61115

The s_i is the coefficient of the following function.

$$f(x,y|s)=s_1x^2y^2+s_2x^2y+s_3x^2+s_4xy^2+s_5xy+s_6x+s_7y^2+s_8y+s_9$$

, wher x and y is local cartesian coordinates (km) from coorindates of an origin 137 °E, 35 °N.

Table 2. Optimum parameters for the 2D basement model.

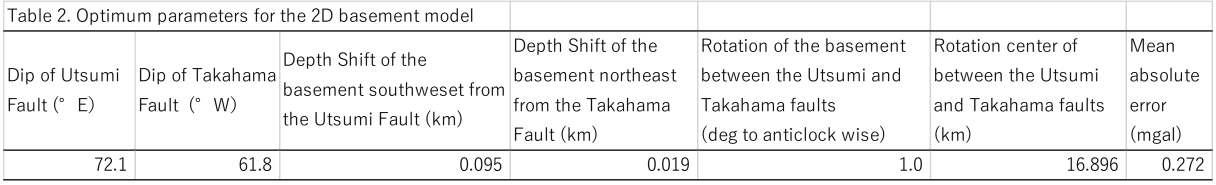

Table 2. Optimum parameters for the 2D basement model

Dip of Utsumi Fault (° E)	Dip of Takahama Fault (° W)	Depth Shift of the basement southweset from the Utsumi Fault (km)	Depth Shift of the basement northeast from the Takahama Fault (km)	Rotation of the basement between the Utsumi and Takahama faults (deg to anticlock wise)	Rotation center of between the Utsumi and Takahama faults (km)	Mean absolute error (mgal)
72.1	61.8	0.095	0.019	1.0	16.896	0.272

Supplementary Table 1. Observed gravity data in the Mikawa Plain, Japan.

Additional Table 1. Observed gravity data in the Mikawa Plain, Japan

No.	Year	Month	Day	Time	Latitude	Longitude	H	Gobs	Gnorm	FAC	BGC	TI	Tw	BGA
1	2018	03	03	0833	345344.3015	1370139.4240	0.813	979742.908	979724.888	1.1208	-0.0342	0.0158	-0.0016	19.0970
2	2018	03	03	0843	345343.5163	1370139.3196	0.835	979742.897	979724.869	1.1276	-0.0352	0.0157	-0.0016	19.1088
3	2018	03	03	0854	345342.6758	1370139.1969	0.862	979742.918	979724.850	1.1359	-0.0363	0.0157	-0.0016	19.1553
4	2018	03	03	0906	345341.7966	1370139.0844	0.864	979742.933	979724.829	1.1365	-0.0364	0.0157	-0.0016	19.1914
5	2018	03	03	0915	345340.9413	1370138.9742	0.805	979742.921	979724.809	1.1183	-0.0339	0.0157	-0.0016	19.1871
6	2018	03	03	0925	345340.0555	1370138.8566	0.749	979742.904	979724.788	1.1011	-0.0316	0.0157	-0.0016	19.1790
7	2018	03	03	0933	345339.1779	1370138.7392	0.704	979742.889	979724.767	1.0872	-0.0297	0.0157	-0.0016	19.1752
8	2018	03	03	0941	345338.3266	1370138.6216	0.694	979742.876	979724.747	1.0841	-0.0292	0.0157	-0.0016	19.1804
9	2018	03	03	0950	345337.4423	1370138.5029	0.656	979742.909	979724.726	1.0724	-0.0276	0.0157	-0.0016	19.2261
10	2018	03	03	1055	345336.5924	1370138.4014	0.586	979742.923	979724.706	1.0508	-0.0247	0.0156	-0.0016	19.2450
11	2018	03	03	1103	345335.7350	1370138.2886	0.650	979742.902	979724.686	1.0705	-0.0274	0.0156	-0.0016	19.2577
12	2018	03	03	1113	345334.8836	1370138.1765	0.602	979742.887	979724.666	1.0557	-0.0254	0.0155	-0.0017	19.2522
13	2018	03	03	1123	345334.6388	1370137.7212	0.742	979742.866	979724.660	1.0989	-0.0313	0.0156	-0.0017	19.2668
14	2018	03	03	1158	345335.1656	1370136.9448	0.731	979742.860	979724.673	1.0955	-0.0308	0.0156	-0.0017	19.2461
15	2018	03	03	1211	345335.0746	1370136.1357	0.627	979742.867	979724.671	1.0634	-0.0264	0.0155	-0.0016	19.2332
16	2018	03	03	1223	345334.4346	1370135.5006	0.584	979742.868	979724.655	1.0502	-0.0246	0.0155	-0.0016	19.2403
17	2018	03	03	1235	345333.8241	1370134.8753	0.622	979742.837	979724.641	1.0619	-0.0262	0.0155	-0.0017	19.2315
18	2018	03	03	1246	345333.1853	1370134.2411	0.541	979742.832	979724.626	1.0369	-0.0228	0.0154	-0.0017	19.2242
19	2018	03	03	1257	345332.5534	1370133.6051	0.662	979742.812	979724.611	1.0742	-0.0279	0.0153	-0.0017	19.2444
20	2018	03	03	1311	345331.9077	1370132.9399	0.776	979742.816	979724.596	1.1094	-0.0327	0.0154	-0.0017	19.2880
21	2018	03	03	1327	345331.2836	1370132.2955	0.793	979742.868	979724.581	1.1146	-0.0334	0.0154	-0.0017	19.3583
22	2018	03	03	1343	345330.6272	1370131.6262	0.776	979742.917	979724.566	1.1094	-0.0327	0.0153	-0.0017	19.4189
23	2018	03	03	1353	345329.9930	1370130.9949	0.833	979742.920	979724.551	1.1270	-0.0351	0.0154	-0.0017	19.4492
24	2018	03	03	1406	345329.3478	1370130.3275	0.887	979742.942	979724.536	1.1436	-0.0374	0.0153	-0.0017	19.4975
25	2018	03	03	1418	345328.7006	1370129.6779	0.884	979742.982	979724.520	1.1427	-0.0372	0.0153	-0.0017	19.5522
26	2018	03	03	1427	345328.0644	1370129.0436	0.943	979743.011	979724.505	1.1609	-0.0397	0.0153	-0.0017	19.6087
27	2018	03	03	1435	345327.4377	1370128.3952	1.004	979743.027	979724.491	1.1797	-0.0423	0.0153	-0.0017	19.6523
28	2018	03	03	1512	345326.7140	1370127.6756	1.119	979743.032	979724.474	1.2152	-0.0471	0.0153	-0.0017	19.6988
29	2018	03	03	1528	345326.0615	1370127.0115	1.166	979743.061	979724.458	1.2297	-0.0491	0.0154	-0.0017	19.7533
30	2018	03	03	1536	345325.4210	1370126.3666	1.223	979743.054	979724.443	1.2473	-0.0515	0.0153	-0.0017	19.7732
31	2018	03	03	1546	345324.8017	1370125.7102	1.270	979743.086	979724.429	1.2618	-0.0535	0.0154	-0.0017	19.8300
32	2018	03	03	1620	345324.1775	1370125.0762	1.336	979743.100	979724.414	1.2822	-0.0563	0.0154	-0.0017	19.8726
33	2018	03	04	0816	345323.5519	1370124.4493	1.342	979743.136	979724.399	1.2840	-0.0565	0.0154	-0.0017	19.9247
34	2018	03	04	0827	345322.9036	1370123.7949	1.401	979743.147	979724.384	1.3022	-0.0590	0.0156	-0.0017	19.9639
35	2018	03	04	0838	345322.2588	1370123.1446	1.477	979743.159	979724.369	1.3257	-0.0622	0.0158	-0.0017	20.0077
36	2018	03	04	0847	345321.6062	1370122.4813	1.529	979743.197	979724.353	1.3417	-0.0644	0.0162	-0.0017	20.0729
37	2018	03	04	0857	345320.9618	1370121.8329	1.672	979743.162	979724.338	1.3858	-0.0704	0.0171	-0.0017	20.0854
38	2018	03	04	0907	345320.3267	1370121.1927	2.069	979743.081	979724.323	1.5083	-0.0872	0.0183	-0.0017	20.1060
39	2018	03	04	0918	345319.0344	1370119.8568	4.636	979742.474	979724.293	2.3002	-0.1953	0.0207	-0.0018	20.0781
40	2018	03	04	0929	345316.7785	1370119.1522	8.877	979741.489	979724.240	3.6086	-0.3739	0.0220	-0.0019	20.0468
41	2018	03	04	0938	345315.7373	1370118.7998	9.401	979741.381	979724.215	3.7702	-0.3960	0.0225	-0.0019	20.0753
42	2018	03	04	1120	345309.1092	1370111.9115	1.953	979743.021	979724.059	1.4725	-0.0823	0.0150	-0.0018	20.2780
43	2018	03	04	1134	345304.9176	1370108.5669	1.800	979742.881	979723.960	1.4253	-0.0758	0.0143	-0.0018	20.2030
44	2018	03	04	1152	345301.4699	1370107.6461	1.649	979742.905	979723.879	1.3787	-0.0695	0.0142	-0.0018	20.2758
45	2018	03	04	1221	345253.5248	1370054.8641	0.916	979742.057	979723.692	1.1526	-0.0386	0.0137	-0.0018	19.4587
46	2018	03	04	1238	345242.0570	1370041.7445	0.904	979741.307	979723.422	1.1489	-0.0381	0.0135	-0.0018	18.9758
47	2018	03	04	1627	345350.3189	1370149.1390	1.570	979743.393	979725.030	1.3544	-0.0661	0.0166	-0.0016	19.6024
48	2018	03	04	1645	345352.1573	1370150.8705	2.395	979743.275	979725.073	1.6089	-0.1009	0.0167	-0.0016	19.6156
49	2018	03	06	1628	345359.0795	1370159.7907	3.961	979743.521	979725.236	2.0920	-0.1669	0.0171	-0.0016	20.0309
50	2018	03	06	1637	345355.4570	1370155.0384	2.097	979743.586	979725.151	1.5169	-0.0883	0.0176	-0.0016	19.7880
51	2018	03	06	1702	345257.6260	1370058.6692	1.300	979742.394	979723.788	1.2711	-0.0548	0.0138	-0.0018	19.7806
52	2018	03	07	0945	345030.7590	1370448.2323	5.439	979750.473	979720.330	2.5479	-0.2291	0.0785	-0.0033	32.3413
53	2018	03	07	1003	345052.8532	1370502.2245	9.259	979750.443	979720.850	3.7264	-0.3900	0.0491	-0.0032	32.5320
54	2018	03	07	1037	344702.7983	1370539.1220	96.056	979729.489	979715.436	30.5029	-4.0431	0.6534	-0.0239	36.7357
55	2018	03	07	1140	344846.6716	1370502.2549	78.979	979732.546	979717.880	25.2348	-3.3248	0.2997	-0.0082	32.9349
56	2018	03	07	1208	344920.5120	1370550.7009	52.508	979739.064	979718.676	17.0687	-2.2109	0.3004	-0.0065	33.0557
57	2018	03	07	1300	345239.7040	1370449.3111	7.477	979752.262	979723.366	3.1767	-0.3149	0.0348	-0.0023	31.4259

Legend

No: Station Number

Year, Month, Day and Time: Obsarevation year month day and time in JST (UTC+9)

Latitude: Latitude (e.g. 242259.9753 means 24 degrees 22 minutes 59.9753 seconds North)

Longitude: Longitude (e.g. 1241000.4210 means 124 degrees 10 minutes 00.4210 seconds East)

H: Observation Point Height (m)

Gobs: Observed gravity value (mGal)

Gnorm: Normal gravity value (mGal)

FAC: Free-air correction value (mGal)

BGC: Bouguer correction value (mGal / 1.0 g/cm^3)

TI: Terrain correction value (mGal / 1.0 g/cm^3)

Tw: Sea water correction value (mGal / 1.0 g/cm^3)

BGA: Bouguer anomaly (assumed density: 2.30 g/cm^3)

Bouguer Anomaly value can be calculated as

$$BGA = Gobs - Gnorm + FAC + (BGC + TI) \times \rho + Tw \times \rho_w$$

where ρ and ρ_w are the assumed densities of surficial rocks and sea water, respectively.

Supplementary Table 2. Elevation of the basement top compiled in this study.

Additional Table 2. Elevation of basement top newly compiled in this study

ID	Longitude (° E)	Latitude (° N)	Basement depth from ground surface (m)	Elevation of ground surface (m)	Elevation of basement top (m)
A1	137.001978	34.9351	470.6	6.7	-463.9
A2	137.06	34.92861	300.78	10.78	-290
A3	137.060567	34.84585	82.81	3.31	-79.5
A4	137.080733	34.789	54.7	1.18	-53.52
A5	137.067464	34.80355	49.11	1.56	-47.55
A6	137.080228	34.87992	51.93	6.33	-45.6
A7	137.066436	34.82022	43.52	1.44	-42.08
A8	137.070511	34.81505	41.98	1.32	-40.66
A9	137.079757	34.88101	46.64	6.44	-40.2
A10	137.100583	34.89916	46.55	10.18	-36.37
A11	137.075233	34.81425	37.8	2.8	-35
A12	137.092697	34.86538	38.35	4.35	-34
A13	137.080592	34.87934	45.32	11.42	-33.9
A14	137.077038	34.81939	33.57	0.75	-32.82
A15	137.079632	34.82069	36.94	4.28	-32.66
A16	137.101131	34.89866	43.11	10.55	-32.56
A17	137.096083	34.86411	36.63	4.93	-31.7
A18	137.096478	34.8634	38.15	7.45	-30.7
A19	137.097168	34.86394	37.67	7.17	-30.5
A20	137.097477	34.86339	35.76	7.76	-28
A21	137.084135	34.85873	31.87	4.87	-27
A22	137.084119	34.85874	31.87	4.91	-26.96
A23	137.096475	34.8579	32	5.23	-26.77
A24	137.097839	34.86312	31.03	4.63	-26.4
A25	137.097267	34.8585	31.41	5.51	-25.9
A26	137.097173	34.85845	31.42	5.52	-25.9
A27	137.068129	34.87436	28.8	6.5	-22.3
A28	137.123886	34.88963	30.73	8.53	-22.2
A29	137.080981	34.8793	29.34	7.94	-21.4
A30	137.065958	34.87378	27.25	5.95	-21.3
A31	137.088295	34.87965	29.02	8.22	-20.8
A32	137.079274	34.88281	25.53	4.83	-20.7
A33	137.083106	34.87296	29.48	9.88	-19.6
A34	137.082364	34.874	36.05	17.45	-18.6
A35	137.100031	34.85583	23.62	5.42	-18.2
A36	137.080686	34.8782	21.62	4.82	-16.8
A37	137.080625	34.87644	24.08	8.08	-16
A38	137.068664	34.87193	17.52	5.22	-12.3
A39	137.076606	34.847	21.82	10.1	-11.72
A40	137.08512	34.82647	15.33	4.45	-10.88
A41	137.068798	34.87265	14.99	4.89	-10.1
A42	137.08029	34.87631	17.71	8.61	-9.1
A43	137.08125	34.87762	17.48	8.68	-8.8
A44	137.08106	34.87708	16.43	8.33	-8.1
A45	137.085389	34.88263	15.56	8.36	-7.2
A46	137.106478	34.89439	13.3	8.09	-5.21
A47	137.080107	34.87626	10.73	6.33	-4.4
A48	137.082204	34.87509	17.11	13.31	-3.8
A49	137.080029	34.87621	11.96	9.36	-2.6
A50	137.08042	34.87543	10.4	8.3	-2.1
A51	137.089061	34.84981	6.84	7.54	0.7
A52	137.088813	34.88242	7.3	9.2	-
A53	137.077603	34.87372	7.57	9.67	-
A54	137.081803	34.87644	12.17	16.87	-
B1	137.00	34.67	0.00	-1.72	-1.72
B2	137.09	34.79	0.00	1.02	-
B3	137.09	34.85	0.00	7.76	-
B4	137.08	34.88	0.00	6.58	-
B5	137.10	34.89	0.00	8.01	-
B6	137.14	34.88	0.00	55.26	-
B7	137.17	34.92	0.00	38.23	-
B8	137.17	35.03	0.00	42.57	-
B9	137.13	35.14	0.00	109.31	-
B10	137.04	35.15	0.00	63.42	-
B11	136.62	35.14	0.00	242.42	-
B12	137.20	34.67	0.00	3.02	-

The data ID with capital A (A1-A54) was derived from the boring cores obtained by Aichi Prefecture and Nishio City.

The data ID with capital B (B1-B12) was derived from the location of the basement rock represented in the geological map.

Supplementary Table 3. Parameters for the 2D basement model calculated from 10 genetic algorithm (GA) experiments.

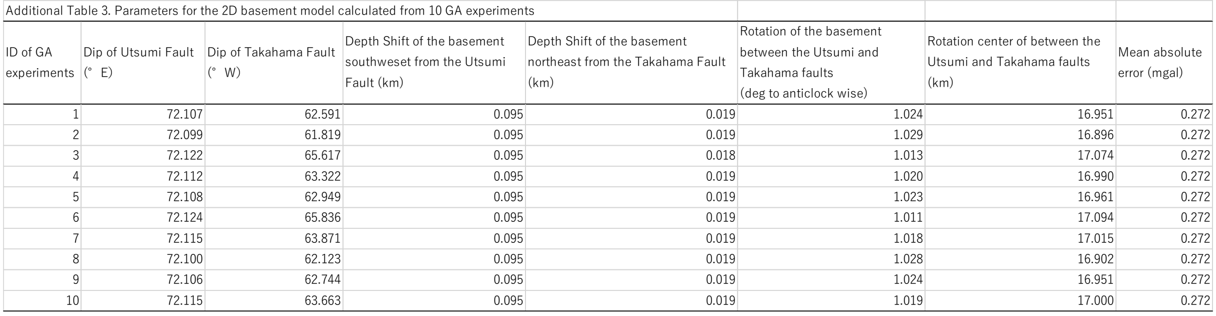

Additional Table 3. Parameters for the 2D basement model calculated from 10 GA experiments

ID of GA experiments	Dip of Utsumi Fault (° E)	Dip of Takahama Fault (° W)	Depth Shift of the basement southweset from the Utsumi Fault (km)	Depth Shift of the basement northeast from the Takahama Fault (km)	Rotation of the basement between the Utsumi and Takahama faults (deg to anticlock wise)	Rotation center of between the Utsumi and Takahama faults (km)	Mean absolute error (mgal)
1	72.107	62.591	0.095	0.019	1.024	16.951	0.272
2	72.099	61.819	0.095	0.019	1.029	16.896	0.272
3	72.122	65.617	0.095	0.018	1.013	17.074	0.272
4	72.112	63.322	0.095	0.019	1.020	16.990	0.272
5	72.108	62.949	0.095	0.019	1.023	16.961	0.272
6	72.124	65.836	0.095	0.019	1.011	17.094	0.272
7	72.115	63.871	0.095	0.019	1.018	17.015	0.272
8	72.100	62.123	0.095	0.019	1.028	16.902	0.272
9	72.106	62.744	0.095	0.019	1.024	16.951	0.272
10	72.115	63.663	0.095	0.019	1.019	17.000	0.272